Segmentation of brain tumors by evidence theory: on the use of the conflict information

A.-S. Capelle, C. Fernandez-Maloigne
Laboratoire SIC - FRE CNRS 2731
Université de Poitiers
Bât. SP2MI, Bd Marie et Pierre Curie
86962 Futuroscope-Chasseneuil, France
capell@sic.univ-poitiers.fr

O. Colot
Laboratoire LAGIS - UMR CNRS 8146
Université des Sciences et Technologies de Lille
Bât. P2, Cité Scientifique
59655 Villeneuve D'Ascq Cedex, France
olivier.colot@univ-lille1.fr

Abstract – *This paper presents an evidential segmentation scheme of multi-echoes magnetic resonance (MR) images for the detection of brain tumors. The segmentation is based on the modeling of the data by evidence theory which is well suited to represent such uncertain and imprecise data. In our approach, the neighborhood relationship between the voxels are taken into account thanks to a weighted Dempster's combination rule. This process leads to a real region-based segmentation of brain and allows the detection of tumors. In this paper we particularly focus on the conflicting information which is generated when combining neighborhood information. We show this conflict reflects the spatial organization of the data: it is higher at the boundary between the different structures. We propose and define a boundary-indicator based on the amount of conflict. This indicator is then used as new source of evidence that the specialist can aggregate with the segmentation results to soften its decision.*

Keywords: Evidence theory, segmentation, neighborhood relationship, conflict information.

1 Introduction

The magnetic resonance (MR) imaging is a grateful tool for the observation of human anatomy. In particular, this engineering has been developed for the study of human brain anatomy and is very useful for the diagnosis of tumors. Indeed, the existence of several MR protocols of acquisition provides different observations of the brain. Each observation usually highlights a particular region of the tumor. Then, to elaborate their diagnosis, the physicians can mentally combine these complementary views and obtain a more complete information about the tumor. Thus, their diagnosis is more accurate and confident.

In this medical context, the processing of MR data is still a challenging problem which usually consists in segmenting the MR images into regions. Each region should then be significant of the anatomical structures and of the tumor location. Numerous methods were proposed to solve the problematic of brain segmentation for the detection of tumors. Mostly, they adopt a multi-echoes point of view in order to take into account numerous, complementary and redundant information [1, 2]. Thus, this is a data fusion problem. The existing segmentation methods are based on various theories. The probability theory is widely used [1, 3–5]. The MR images are often modeled by gaussian mixtures probability functions. Then, the main difficulty is to properly estimate these probability density functions. Let us denote that is not obvious that the tumor can be modeled by a gaussian process. Then, some authors detect the tumor as outliers with respect to a statistical model for normal brain MR images [6]. Others segmentation methods are based on fuzzy sets [7]. In particular, one finds several versions of the Fuzzy-C-Means (FCM) clustering algorithm [8] (automatic [9], semi-automatic [10], including *a priori* knowledge [11]). Whereas these methods are simple and fast, their efficiency depends on the quality of MR images and are particularly sensitive to noise.

In order to take into account the imprecision and the uncertainty of MR images, we propose the use of evidence theory [12,13] which is well suited to treat such imperfect data. Moreover, this theory provides combination tools to merge data issued from several sources (MR acquisition protocols) while taking into account their complementarity, their redundancy and their possible opposition. Thus, this theory is convenient to a multi-echoes segmentation approach.

Our segmentation scheme [14] is based on the use of evidence theory. One of its characteristics is to take into account the spatial dependency between the voxels through an evidential spatial merging process. This process consists in considering each spatial neighbor as an information source. In a particular neighborhood, the combination of the information brought by each voxel globally increases the knowledge. Finally, this process leads to a real region-based segmentation of the brain.

In this paper, we focus on the study of the conflict generated by the spatial combination process. In particular, we show this conflicting mass brings some information about the location of the boundaries between the different brain structures. Moreover, we propose its use for the interpretation of the segmentation results.

This paper is divided as follow. In Section 2, we present the main aspects of evidence theory. In Section 3 we describe the evidential segmentation scheme and its application to multi-echoes MR images segmentation. In Section 4, we study and analyze the conflicting information and we propose the definition of a boundary-indicator based on the use of the conflicting information. In Section 5, we conclude and propose some new developments.

2 Evidence theory background

In this section, we describe theoretical background of evidence theory.
Evidence theory, or theory of belief structures, was initially introduced by Dempster's works on the concepts of lower and upper bounds for a set of compatible probability distributions [12]. In [13], Shafer formalized the theory and showed the advantage of using belief structures to model imprecise and uncertain data. Different interpretations of the native "Dempster-Shafer" theory successively appeared [15]. Smets and Kennes [16] deviate from the initial probabilistic interpretation of the evidence theory with the *Transferable Belief Model* (TBM) giving a clear and coherent interpretation of the underlying concept of the theory.

2.1 Belief structures

We suppose the definition of a set of hypotheses Ω called frame of discernment, defined as follow:

$$\Omega = \{H_1, \ldots, H_n, \ldots, H_N\}\,. \tag{1}$$

It is composed of N exhaustive and exclusive hypotheses. From the frame of discernment, let 2^Ω be the power set composed with the 2^N propositions A of Ω:

$$\begin{aligned} 2^\Omega \;=\; & \{\emptyset, \{H_1\}, \{H_2\}, \ldots, \{H_N\}, \{H_1 \cap H_2\}, \\ & \{H_1 \cap H_3\}, \ldots, \Omega\}\,. \end{aligned} \tag{2}$$

The piece of evidence brought by a source of information (sensor, agent...) on a proposition A (singleton or composed hypothesis of 2^Ω), is modeled by the belief structure m, called Basic Belief Assignment (bba), defined by:

$$m : 2^\Omega \rightarrow [0, 1], \tag{3}$$

and verifying:

$$m(\emptyset) = 0, \tag{4}$$

$$\sum_{A \subseteq \Omega} m(A) = 1. \tag{5}$$

From this function, two belief structures, the credibility (Bel) and the plausibility (Pl) can be derived by the following equations:

$$Bel(A) = \sum_{B \subseteq A} m(B), \tag{6}$$

$$Pl(A) = \sum_{A \cap B \neq \emptyset} m(B). \tag{7}$$

The degree of belief $Bel(A)$ can be interpreted as the total amount of belief in the proposition A. The plausibility $Pl(A)$ quantifies the maximum amount of belief potentially attributed to A. The credibility and the plausibility are thus dual notions: the plausibility is defined by $Pl(A) = Bel(\Omega) - Bel(\overline{A})$ where $\overline{A}$ is the complementary of A.

2.2 Belief attenuation

The belief structure m models the piece of evidence brought by a source of information on the different hypotheses of 2^Ω. When this source is considered as imprecise or not completely reliable, the confidence in this source can be attenuated by a factor α and a derived belief structure m_α is then defined by:

$$m^\alpha(A) \;=\; \alpha.m(A) \quad \forall A \in 2^\Omega, \tag{8}$$

$$m^\alpha(\Omega) \;=\; 1 - \alpha + \alpha.m(\Omega). \tag{9}$$

The difficulty lies then in the correct definition of the factor α [17].

2.3 Combination

Let denote $\{m_1, \ldots, m_J\}$ J belief structures associated to J independent sources $S_1, \ldots, S_J$ of information. The evidence theory provides an adapted framework to fusion or combine these J sources in a synthesized information. A common operator is the orthogonal sum also called the Dempster's combination. Thus, the merged belief structure $m_\oplus$ is defined by:

$$m_\oplus = m_1 \oplus \ldots \oplus m_j \oplus \ldots m_J\,. \tag{10}$$

For two sources of information S_1 and S_2, the merged belief structure $m_\oplus$ is given by:

$$\forall A \subseteq \Omega \quad m_\oplus(A) = \frac{1}{1-k} \sum_{B \cap C = A} m_1(B).m_2(C), \tag{11}$$

where k is defined by:

$$k = \sum_{B \cap C = \emptyset} m(B).m(C)\,. \tag{12}$$

The normalization term k, with $0 \leq k \leq 1$, can be interpreted as a measure of the conflict between the sources to combine. The Dempster's combination rule has been justified theoretically by several authors [18, 19]. However the normalization step was also criticized [17, 19]. It is very important to take into account the value of this term: when k is high (≈ 1), combining the sources is a non-sense leading to incoherence and involving counter-intuitive behaviors [17, 20] .

2.4 Decision

For most applications, a decision has generally to be taken in favor of a simple hypothesis. Within the context of the TBM, Smets defines and justifies the use of the pignistic decision rule [16].
Let $BetP$ be the pignistic probability distribution derived from the belief structure m. $BetP$ is defined by:

$$BetP(H_n) = \sum_{A \subseteq \Omega,\ H_n \in A} \frac{m(A)}{|A|.(1 - m(\emptyset))} \quad \forall H_n \in \Omega\,, \tag{13}$$

where $|A|$ is the cardinality of A.

Let us denote X a pattern to be assigned in one of the N hypotheses of the frame of discernment Ω. We denote $\{a_1, \ldots, a_N\}$ the set of all the possible actions, where $a_{i,\, i=1,\ldots,N}$ is the decision to assign X to H_i. We name $\lambda(a_i|H_j)$ the cost of deciding a_i whereas X belongs to H_j. If we consider the simplest case where the losses are assumed to be equal to 1 for misclassification and 0 for correct classification ($\lambda(a_i|H_j) = 1 - \delta_{i,j}$), the pignistic decision rule is writen as:

$$D_{BetP}(X) = a_i \quad \text{with} \quad a_i = \arg\max_{H_j \in\, \Omega} \; BetP(H_j)\;. \tag{14}$$

Let us denote that a rejection class can be introduced in the decision step.

3 Segmentation scheme

In this section, we describe the evidential segmentation scheme and its application on multi-echoes MR data. Let us denote that the reader can refer to [14] for more details. The objective of this process is to divide the MR data volume into regions significant of the main anatomical structures in order to detect and locate the tumors.

3.1 Notations

Let p be the number of used echoes and $X = [x_1, \ldots, x_p]$ a particular pattern to classify. x_i represents the gray level associated with the echo i. The frame of discernment Ω is composed of the hypotheses $H_{i,\, i=1,\ldots,N}$ where N is arbitrary fixed. Usually, $N = 5$ and one hypothesis corresponds to a particular anatomical structure among the white matter (WM), the grey matter (GM) and the cerebrospinal fluid (CF), the tumor (T) and the œdema (O).

3.2 Segmentation scheme description

The segmentation scheme is divided into three steps:

1. *Classification step:* each pattern X is associated with a belief structure m with respect to a particular evidential model;
2. *Segmentation step:* for each pattern X, spatial neighborhood information is integrated via a weighted Dempster's combination rule;
3. *Decision step:* for each pattern X, a decision a_i is taken using Eq. (14). Then, the MR volume is segmented into regions.

3.2.1 Classification step

The classification step's objective is to associate a belief structure m to each pattern X in respect with an evidential model. Generally, the models depend upon the classification problem. Preliminary searches [14] showed that the distance-based model defined by Denœux [21] is very convenient in our application. This model is the one used thereafter.

The distance-based model can be considered as an evidence-theoretic K-NN rule. Let $\mathcal{T}$ be a training set composed of couples $\{X^s, H_q\}$ where H_q is the hypothesis associated with the pattern X^s. Moreover, let ω_q be the prototype which represents all the training patterns assigned to $H_q \in \Omega$.
The distance-based model supposes that each neighboring couple $\{X^k, H_s\} \in \mathcal{T}$ of X brings some useful information to determine the class membership of X. This information is modeled by a belief structure m_k defined by:

$$\left\{ \begin{array}{lcl} m_k(\{H_s\}) & = & \eta\,.\exp\{-\gamma_s\,.\,d(\omega_s, X)^2\} \\ m_k(\Omega) & = & 1 - \eta\,.\exp\{-\gamma_s\,.\,d(\omega_s, X)^2\} \\ m_k(A) & = & 0, \forall A \neq H_s, A \subsetneq \Omega \end{array} \right. , \tag{15}$$

where $0 \leq \eta \leq 1$ is a constant, $d(\omega_s, X)$ is the Mahanalobis distance between the pattern X and the prototype ω_s and $\gamma_s \in \mathbb{R}^+$ adjusts the influence on the prototype ω_s [22].
Considering K independent neighbors, the belief structure m associated with X is obtained by merging the K belief structures m_k with $k = 1, \ldots, K$ by means of the Dempster's combination rule:

$$m = m_1 \oplus \ldots m_k \oplus \ldots \oplus m_K\,. \tag{16}$$

An important key point is obviously the definition of the training set $\mathcal{T}$. We propose to initially model the MR data volume by a gaussian mixture. The parameters (mean and variance) of each normal distribution are then estimated by the Expectation-Maximization (EM) [23] algorithm. Each couple (mean, variance) is then associated with a prototype $\omega_{i,\, i=1,\ldots,N}$.
Once we have determined the belief structures for all the pattern X, it is already possible to obtain a classification of the MR volume using the pignistic decision rule. However, this classification does not take into account the spatially order which exists between voxels. These relationships are including in the *segmentation step*.

3.2.2 Segmentation step

The basic idea is to take into account the spatial order and the correlations which exist between the voxels of the volume. Thus, we consider each neighbor of a pattern X brings some information useful to identify the class membership of X. Let ∂_X be a particular neighborhood of X, composed of M voxels:

$$\partial_X = \{X_1, \ldots, X_M\}\,. \tag{17}$$

Usually we consider the 26-connex neighborhood (M=26). Moreover, let $m_{i,\, i=1,\ldots,M}$ be the belief structures associated with $X_{i,\, i=1,\ldots,M}$ obtained using Eqs. (15-16). It is obvious that the influence of a neighbor depends on its distance to the voxel X: the larger the distance is, the weaker should be its influence. Thus, we propose to discount the belief structure m_i by means of a coefficient α_i where $0 \leq \alpha_i < 1$ depends on the Euclidean distance d_ε between X_i and X. Then, we propose:

$$\alpha_i = \exp\{-\beta\,.\,d_\varepsilon^2(X, X_i)\}\,, \tag{18}$$

where $\beta \in \mathbb{R}^+$. Our study shows that β has to be in the range $[0.5; 1.5]$. Heuristic results give $\beta = 0.6$ as a good compromise.
Finally, the belief structure m' associated with X is given by:

$$m' = m \oplus m_1^{\alpha_1} \oplus \dots m_M^{\alpha_M} . \quad (19)$$

3.2.3 *Decision step*

Decision making is last step of the segmentation scheme and consists in determining the class membership of each voxel of the MR volume. We use the pignistic decision rule (Eq. (14)) which is the one justified using TBM [16].

3.3 Application to MR data volumes

This short part describes some segmentation results obtained with the proposed segmentation scheme. This method was applied both on simulated normal brain volumes issued from the *BrainWeb* database [24] and on real data volumes issued from the Regional University Hospital Center of Poitiers (CHRU).

3.3.1 *Simulated MR data volume*

The main advantage of using simulated volumes is that we perfectly know the characteristics of the images (noise level (n), radiofrequency bias field intensity level (rf)) and the class membership of each voxel. The multi-echoes volumes are composed of a T_1-weighted, a T_2-weighted and a PD-weighted echoes (p=3). For each volume, a voxel sizes $1 \times 1 \times 1$ millimeter. The frame of discernment is defined by $\Omega = \{H_{WM}, H_{GM}, H_{CF}\}$ (N=3). The volume presented Fig. (1) is corrupted by some noise ($n = 3\%$) and a bias field ($rf = 20\%$).

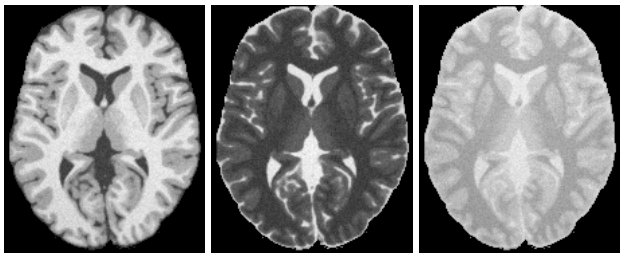

(a) T_1 (b) T_2 (c) PD

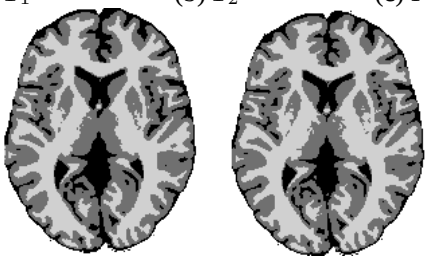

(d) segmentation result (e) ground truth

Fig. 1: One slice of the simulated data volume

Comparing the segmentation result Fig. (1-d) and the ground truth Fig. (1-e), we observe the efficiency of the segmentation method. The visual results are confirmed by the segmentation error rate on the volume (ξ) which is equal to 4.04%. This same volume segmented with the EM algorithm followed by a regularization by an Iterated Conditional Modes (ICM) algorithm provides an error rate equal to 6.01%. The Tab. (1) presents the results obtained for all the volumes of the database. The evidential segmentation scheme is denoted EV. We can observe the advantage of using an evidential scheme comparing to a probabilistic scheme.

ξ (%)	$n = 3\%$			$n = 5\%$		
rf	0%	20%	40%	0%	20%	40%
EV	4.04	6.20	11.48	6.75	5.55	13.13
ICM	6.01	6.63	14.48	6.48	5.68	14.59

	$n = 7\%$			$n = 9\%$		
rf	0%	20%	40%	0%	20%	40%
EV	5.53	6.10	14.53	7.10	9.59	16.71
ICM	5.73	6.53	17.49	7.50	10.28	18.85

Table 1: Error rates on the BrainWeb database

3.3.2 *Real MR data volumes*

For clarity, we only propose in this section the results obtained on one MR data volume[1]. This volume is composed of a T_1Gado[2]-weighted and a T_2-weighted echoes (p=2). A slice of each echo is represented Fig. (2-(a,b)). A voxel sizes $0.94 \times 0.94 \times 1.2$ millimeter and the volume is composed of $256 \times 256 \times 89$ voxels. The frame of discernment is defined by $\Omega = \{H_{WM}, H_{GM}, H_{CF}, H_T, H_O\}$ (N=5).

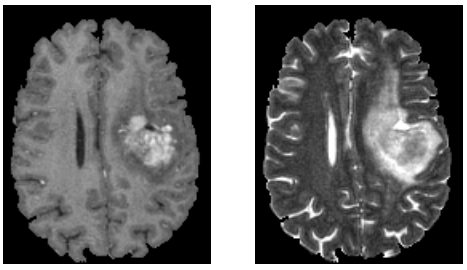

(a) T_1 (b) T_2

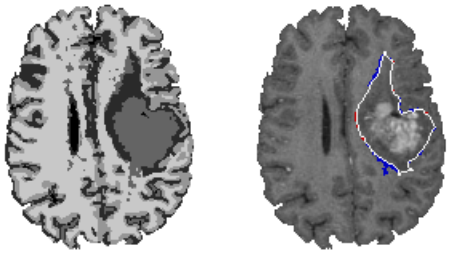

(c) segmentation result (d) medical expertise

Fig. 2: One slice of the real data volume

[1]Ten MR data volumes have been segmented at this time.

[2]The T_1Gado-weighted image is obtained using a contrast product, the Gadolinium.

On Fig. (2-c), we observe that the anatomical structures are found (from lighter to darker, we find the WM, the GM, the T, the O and the CF). The Fig. (2-d), represents the medical expertise of the segmentation: we compare the estimated regions corresponding to the œdema and to the tumor with the ones manually defined by an expert. The red regions corresponds to non-detection (ND), the blue ones corresponds to false-alarm (FA) and the white line corresponds to well-detection (WD). On the whole volume, the WD rate is equal to 96.54%, the ND rate is equal to 3.46% and the FA rate is equal to 8.15%. These rates emphasize the good efficiency of the method. The results were confirmed with 10 other real volumes.

4 Conflict information

We have proposed a segmentation scheme and showed its efficiency to divide multi-echoes MR images into regions which are significant of the brain structures. In this part, we are interested in the conflicting mass and, in particular, on the conflict generated during the *segmentation step* by the combination of neighboring belief structures.

4.1 Origins and meaning

4.1.1 General case

As shown in Eqs. (11, 12), the conflicting mass, denoted k and such as $0 \leq k \leq 1$, appears when combining belief structures. It reflects the level of opposition which exists between the information sources. Three main reasons explain its presence [20]:

- The first is an aberrant measurement given by a sensor; abnormal measurement (denoted outliers in pattern recognition applications) can generate a conflicting mass during the combination.
- The second reason relies on the definition of the belief model. Thus, the use of an imprecise or an inappropriate belief model may provide a conflicting mass.
- Finally, when the information sources to aggregate are numerous, a conflicting mass can be induced even if these sources agree.

Solutions are proposed to manage the conflict problem through several combination rules. These rules are divided in two classes. The first one supposes that the sources are reliable. Thus, the combination operators which can be derived are conjunctive (Dempster [12], Smets [16]). The second class states that one information source tell the truth but without knowing exactly which of them. Thus, the combination operators are mainly disjunctive (Yager [25], Dubois-Prade [26]).

4.1.2 Spatial conflict

During the *segmentation step*, we introduce the spatial information brought by the neighbors through out a weighted Dempster's combination rule. This mechanism obviously generates a conflicting mass. The Fig. (3) represents the

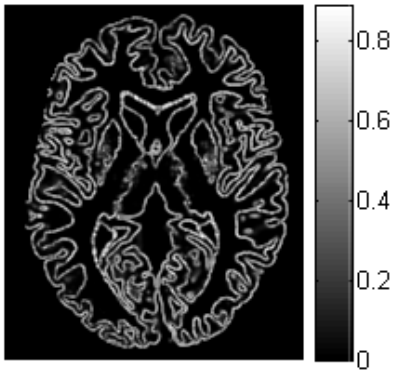

(a) conflict of the simulated slice

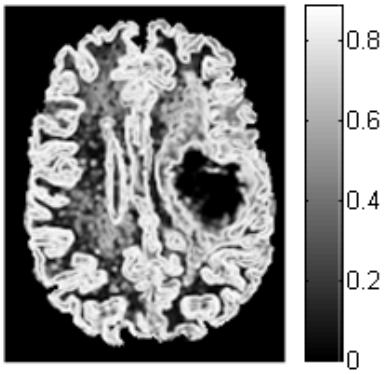

(b) conflict of the real slice

Fig. 3: Conflicting images

conflicting images corresponding to the two MR slices presented above. The conflicting mass scales from 0 to 1.
On the Fig. (3), we observe that the conflict distribution is very specific; the conflicting mass is mainly concentrated on the boundary between the different anatomical structures. This characteristic can be explained by two particular situations existing when combining the neighboring belief structures:

- *Inside a region*: when the spatial combination is done inside a region, the majority of the belief structures supports the same hypothesis. The information sources agree and generate a low conflicting mass (dark points in the images). Let us denote that if one of the neighboring voxel is corrupted by noise, the others neighbors, which are more numerous, rectify the false belief. The spatial combination acts as a spatial filtering which can be considered as a denoising process of the images.
- *At the boundary between structures*: when the spatial combination is done at the boundary between different anatomical structures, all the belief structures does not support the same hypothesis. For example, one part supports the hypothesis H_{WM} whereas the other part supports hypothesis H_{GM}. Thus, their opposition generates a high conflict (light points in the conflict images) which is significant of a presence of the boundary between the structures.

These two particular situations explain that the conflicting mass is mainly localized at the boundary between the struc-

tures and that it is low inside the region corresponding to the anatomical structures. In order to illustrate this characteristic, we have extracted from the ground truth of the simulated brain, the true boundaries between the WM and the GM. Then, we have superposed these boundaries upon the conflicting mass obtained at the end of the segmentation process. The result is represented Fig. (4). The true boundaries are drawn in red. As we can see, the true boundaries and the maxima of the conflicting mass perfectly match.

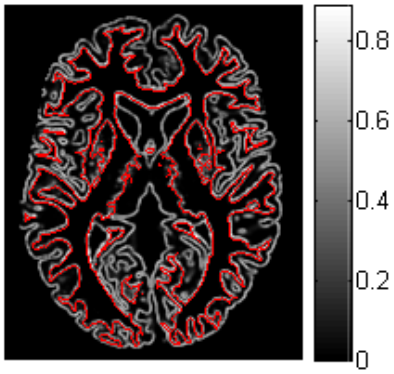

Fig. 4: True boundaries between the WM and the GM (in red) superposed upon the conflicting images

However, on the Fig. (3-b), which corresponds to the conflicting slice of a real volume, we observe that conflict of mid-intensity is located within the anatomical regions too (see the regions corresponding to the WM). We explain the presence of such a conflict by the imprecision of the belief model. Indeed, it is more difficult to precisely estimate the models parameters of a real volume which is composed of more classes than the simulated volume and which is usually corrupted by noise. The training imprecision induces conflicting masses because of the elementary belief structures combination (Eq. (16)). Thus, this initial conflicting mass is still present at the end of the segmentation process: the final conflict (Fig. 3) is composed of the conflict coming from the initial modeling and of the conflict issued from the spatial combination. We have to be very careful when analyzing the final conflict.

4.2 Conflict and boundary localization

On the Fig. (3) and (4), we have observed that the distribution of the conflicting mass is correlated to the location of the boundaries between the different anatomical structures. This link indicates that the conflicting masses are informative data and we propose to use the conflicting masses to define an indicator about the boundary location. Let $c(X)$ be the intensity of the conflict associated to the pattern X. Thus, we define the boundary-indicator $\mathbb{I}(X)$ associated to X by:

$$\mathbb{I}(X) = \begin{cases} 0 & \text{if } c(X) < \lambda_c \\ c(X) & \text{if } c(X) \geq \lambda_c \end{cases} , \qquad (20)$$

where $0 \leq \lambda_c \leq 1$ is a constant threshold. When $c(X) < \lambda_c$, we consider that the conflict is to weak to be significant of the presence of a boundary. On the contrary, when $c(X) \geq \lambda_c$, two situations are possible. In the first case, the pattern X is located near or on a boundary. In the second case, the high conflict is due to the presence of noise or due to an imprecise training.

If we apply the Eq.(20) to all the voxels of the MR volume, we obtain a boundary-indicator, denoted $\mathbb{I}$, which reflects the probable location of the boundaries between anatomical structures. Obviously, the use and the interpretation of $\mathbb{I}$ depend on the relevance of the threshold λ_c.

Experiments made on different simulated and real MR volumes have shown that the value $\lambda_c = \mu_c + 0.2\,\sigma_c$, where μ_c is the mean conflict on a MR volume and σ_c^2 its variance, provides a boundary-indicator coherent compared to the content of the data (Fig (5)). We notice that the residual conflicting lines match with the transitions between the different structures. The observation of this image is sufficient to provide a good representation of the content of the initial images.

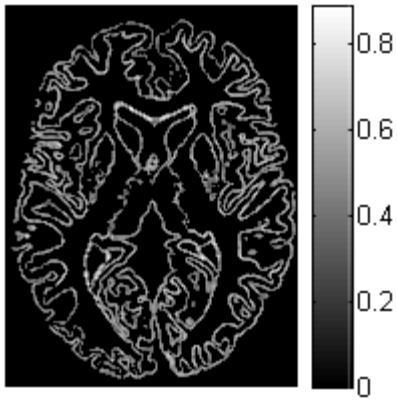

(a) simulated slice

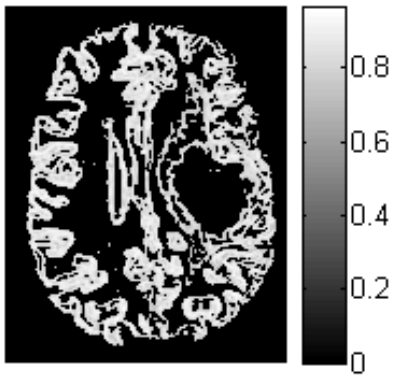

(b) real slice

Fig. 5: boundary-indicator ($\lambda_c = \mu_c + 0.2\,\sigma_c$)

Thus, we propose to use this *boundary* information to complete the results obtained by the previously described segmentation scheme which is a *region* segmentation process. In particular, the contour information can be used by physician when they analyze the segmentation results. Within the context of the aid to decision making, the observation of such an image can help to adjust the belief about the location of tumoral regions.

5 Conclusion

In this paper, we propose an evidential segmentation scheme dedicated to multi-echoes MR volumes in order to detect brain tumors. The method combines the modeling of the knowledge by means of evidence theory and integrates the spatial dependency between the voxels. The modeling via evidence theory allows to take into account the characteristics of the multi-echoes MR images: complementarity, redundancy and incompleteness. Moreover, evidence theory brings the theoretical support and tools for the combination of such information. The introduction of spatial dependency makes it possible to obtain, not only a classification process, but a real segmentation process.

At first, we have described the evidence theory background and the segmentation scheme. This one is characterized by the modeling of the knowledge by a distance-based model which realizes a classification step. Including the neighborhood relationship between the voxels by a weighted Dempsters combination rule, we obtain a real segmentation process. The efficiency of such a method is shown through out the segmentation of simulated MR normal brain volumes and the segmentation of real MR brain volumes presenting a tumor.

The main contribution of our work deals with the analysis and the interpretation of the conflicting mass. We show that the conflict generated by the spatial combination of the belief structures is a useful and significant information. It is not only a consequence of data fusion but it is also an information source about the spatial organization of the data. Thus, we propose and define an indicator, called *boundary-indicator*, which indicates the possible location of the boundaries between the different anatomical structures. Within the context of the aid of diagnosis, this information can be used by specialists. In particular, it allows to soften the results provided by the segmentation in regions.

Currently, we continue our investigations in analyzing the conflicting information and on its integration in the segmentation process. It should allow to obtain a complete segmentation scheme including both region and contour approaches. This should increase the quality and the confidence of the segmentation results.

References

[1] J.C. Bezdek, L.O. Hall, and L.P. Clarke. Review of mr image segmentation techniques using pattern recognition. *Medical Physics*, 20(4):1033–1048, Jul/Aug 1993.

[2] A. Zijdenbos and B.M. Dawant. Brain segmentation and white matter lesion detection in mr images. *Critical Reviews in Biomedical Engineering*, 22(5/6):401–465, 1994.

[3] T. Géraud. *Segmentation des structures internes du cerveau en imagerie par résonance magnétique tridimensionnelle*. PhD thesis, École Nationale Supérieure des Télécommunications, 1998.

[4] G. Gerig, J. Martin, R. Kikinis, O. Kbler, M. Shenton, and F.A. Jolesz. Unsupervised tissue type segmentation of 3d dual-echo mr head data. *Image and Vision Computing*, 10:349–360, 1992.

[5] A. Zijdenbos, R. Forghani, and A. Evans. Automatic quantification of MS lesions in 3D MRI brain data sets: Validation of INSECT. In Springer LNCS, editor, *MICCAI*, volume 1496, pages 439–448, 1998.

[6] K. Van Leemput, F. Maes, D. Vandermeulen, A. Colchester, and P. Suetens. Automated Segmentation of Multiple Sclerosis Lesions by Model Outlier Detection. Technical report, Katholieke Univ. Leuven, 2000.

[7] L.A. Zadeh. Fuzzy sets. *Information and Control*, 8:338–353, 1965.

[8] J.C. Bezdek. Pattern recognition with fuzzy objective functions algorithms. *Plenum Press*, 1981.

[9] R.P. Velthuizen, L.P. Clarke, S. Phuphanich, L.O. Hall, A.M. Bensaid, J.A. Arrington, H. Greenberg, and M. Silbiger. Unsupervised measurement of brain tumor volume on mr images. *JMRI*, 5(5):594–605, 1995.

[10] M. Vaidyanathan, L.P. Clarke, R.P. Velthuizen, S. PhuPhanich, A.M. Bensaid, L.O. Hall, J.C. Bezdek, A. Trotti, and M. Silbiger. Comparison of supervised mri segmentation methods for tumor volume determination during therapy. *Magnetic Resonance Imaging*, 13(5):719–725, 1995.

[11] M.C. Clark, L.O. Hall, D. Goldgof, R. Velthuizen, F. Murtagh, and M. Silbiger. Automatic tumor segmentation using knowledge-based techniques. *IEEE Trans. on Medical Imaging*, 17(2):187–201, 1998.

[12] A. Dempster. Upper and lower probabilities induced by multivalued mapping. *Annals of Mathematical Statistics*, 38:325–339, 1967.

[13] G. Shafer. *A Mathematical Theory of Evidence*. Princetown Univ. Press, 1976. Princetown New Jersey.

[14] A.-S. Capelle, O. Colot, and C. Fernandez-Maloigne. Evidential segmentation scheme of multi-echo mr images for the detection of brain tumors using neighborhood information. *Information Fusion*, 2004. To be published.

[15] P. Smets. What is Dempster-Shafer's model ? In *Advances in the Dempster-Shafer Theory of Evidence, R.R. Yager, M. Fedrizzi and J. Kacprzyk edition*, pages 5–34, New York.

[16] P. Smets and R. Kennes. The transferable belief model. *Artificial Intelligence*, 66(2):191–234, 1994.

[17] L.A. Zadeh. *On the Validity of Dempster's Rule of Combination of Evidence*. Univ. California, Berkeley, 1979. ERL Memo M79/24.

[18] D. Dubois and H. Prade. On the unicity of Dempster rule of combination. *Int. J. Intelligent System*, pages 133–142, 1996.

[19] F. Voorbraak. On the justification of Dempster's rule of combination. *Artificial Intelligence*, pages 171–197, 1991.

[20] E. Lefevre, O. Colot, and P. Vannoorenberghe. Belief function combination and conflict management. *Information Fusion*, pages 149–162, 2002.

[21] L.M. Zouhal and T. Denœux. An adaptative k-NN rule based on Dempster-Shafer theory. In *6th Int. Conf. Computer Analysis of Images and Pattern*, pages 310–317, September 1995.

[22] L.M. Zouhal and T. Denœux. An evidence-theoretic k-nn rule with parameter optimization. *IEEE Trans. Systems, Man and Cybernetics*, 28:263–271, 1998.

[23] A. Dempster, N. Laird, and D. Rubin. Maximum likelihood from incomplete data via the em algorithm. *J. Royal Statistical Society*, 39:1–38, 1977.

[24] C.A. Cocosco, V. Kollokian, R.K.-S. Kwan, and A.C. Evans. Brainweb: Online interface to a 3d mri simulated brain database. *NeuroImage*, 5, 1997. http://www.bic.mni.mcgill.ca/brainweb/.

[25] R.R. Yager. On the Dempster-Shafer framework and new combination rules. *Information Sciences*, 41:93–137, 1987.

[26] D. Dubois and H. Prade. Representation and combination of uncertainty with belief function and possibility measures. *Computer Intelligence*, 1988.